A New Model for the Recovery of Cylindrical Structures from Medical Image Data

Thomas O'Donnell[1] Alok Gupta[1] and Terrance Boult[2]

[1] Siemens Corp Research, Inc. 755 College Road East Princeton, NJ 08540 {odonnell;alok}@scr.siemens.com
[2] Dept. of Computer Science Lehigh University Bethlehem, PA 18015 tboult@eecs.lehigh.edu

Abstract. We introduce a novel analytic model formulation for recovering cylindrical structures (e.g., blood vessels) from segmented 3-D medical image data. Unlike all previous formulations, our model is capable of describing a cylinder with an arbitrary spine (a space curve based on cubic B-splines) and arbitrary cross section which is guaranteed to be orthogonal to the spine. Given this expressiveness, we are able to provide a second order continuous approximation to the centerline of nearly any tubular object. This information may be used for such tasks as a reformatting of the original image data in order to visually detect stenoses or aneurysms. In addition, the cross-section parameter values of our model may aid in *automatically* isolating these regions. We maintain a relatively simple cross-section function to make this detection straightforward (note that any cross-section function is possible). To describe fine detail in the data, we employ local finite element deformations from the model surface. Thus we are able to recover gross geometric approximations as well as quantify characteristics of the object such as its surface area. We apply our model to the recovery of both a healthy and diseased aorta from segmented CT acquisitions.

1 Introduction

Cylindrical structures are very common in the body. Vessels, bones, and intestines for example, are all primarily tubular in shape. In order to provide quantification and analysis of these structures, flexible accurate models become very useful. In medical imaging applications, such models allow for the construction of a 3-D representation of an object from a series of 2-D image slices. This 3-D representation may now be more easily manipulated to understand the object's structure, or serve as the basis for virtual fly-throughs. Such models may also facilitate the measurement of changes in structure over time (e.g., due to calcifications) or detect abnormalities such as unnatural narrowing or ballooning. Finally, in the creation of prosthetic tubular structures, reliable cylindrical models are essential for proper design.

In this paper we present a novel cylindrical model formulation and demonstrate its ability to recover human aorta from segmented medical image data. The model is a form of Generalized Cylinder (GC). That is, it may be thought of

as a cross-section swept along a path (the spine) to create a volume. Our spine is described by a 3-D cubic B-spline and our cross-section function is always plotted in the plane orthogonal to the spine. We augment our model with finite element (FEM) mesh deformations from the surface to express fine detail.

The strength of our formulation is threefold. First, the model is very general. By basing the spine on cubic B-splines, we can create a cylinder which follows almost any space curve. Along this space curve we calculate a continuous trihedral frame. Since the frame is continuous, the cross-section plotted on it is free to be *any* shape and may change along the spine. For the experiments described in this paper we have chosen a variable elliptic cross-section. Fine detail (common in complex anatomical structures) unaddressed by the model directly may be realized by an additional FEM mesh-like component lying atop it. The inclusion of this component allows us to make quantitative statements about the object under study (e.g., reporting its surface area).

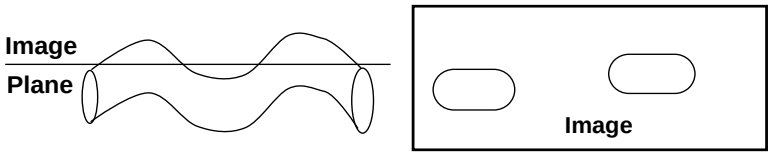

Fig. 1. Left: A vessel and an image plane intersecting it. Right: the resulting image. Based on such a viewpoint it is difficult to detect stenoses or aneurysms.

Second, our model's cross-section is always in the plane orthogonal to the spine. This automatically provides the information for appropriate planar reformatting of an image set and is especially useful for vessels which have been imaged in-plane (see Figure 1). Also, measurements of vessel diameter become possible since the proper plane in which to make the measurements is known (see Figure 2).

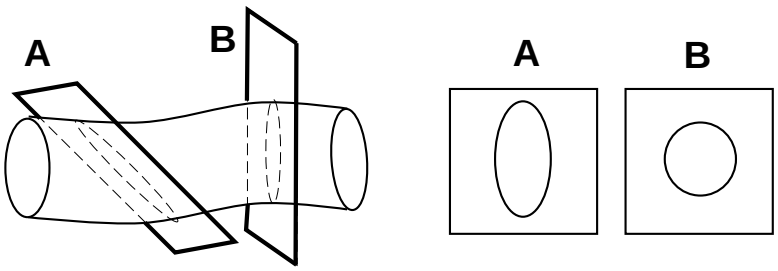

Fig. 2. Left: Vessel with two cross-sectional cuts. Right A: image resulting from a plane not orthogonal to the spine. The vessel's diameter is distorted. Right B: image resulting from cutting in the plane orthogonal to the spine. The true diameter of the vessel may be inferred.

Third, since we have parameters describing the radius of the model, changes

in vessel diameter may be automatically detected. Thus, locations of possible stenoses or aneurysms may be isolated. Other aspects of the cross-section may be addressed by simply incorporating them into the cross-section function to be recovered.

We will see that in the combination of these three aspects, particularly the first two, our model formulation is different from any currently existing. In the next section we will draw comparisons with other cylinder model formulations. Following this we will describe our formulation in more detail and show results of our experiments verifying its effectiveness. Finally, we will draw conclusions on our work and present future directions.

2 Related Work

Stockman and Huang [3] introduced a form of general axis GC dubbed the "the tube description." The model sets up an object-centered coordinate frame with a cross-section function free to rotate with respect to it. The tube model is elegant and flexible, but the cross-section function is not kept orthogonal or even at a constant angle with respect to the spine.

A more common cylinder representation is based on the Frenet-Serret formulae [9]. The moving trihedron formed by the tangent, normal and binormal vectors defined by these formulae may serve as the foundation for a cross-section along a space curve. In contrast to the tube description, Frenet-Serret based models are guaranteed to have their cross-sections orthogonal to the spine.

However, the Frenet-Serret based formulation has three major drawbacks. The first, and simplest, is that it cannot describe a GC with a linear spine because the normal vector is no longer well-defined. The second drawback is related to the first. The formulation cannot describe GCs which are linear at *any* point along the spine; this includes inflection points where the spine is locally straight. The cylinder is discontinuous at these points (Figure 3). And, if the curvature of the spine changes sign the orientation of the trihedral frame instantaneously flips, complicating any simple scheme to interpolate over it. Considering that inflection points appear frequently in common spine functions (e.g polynomials, trigonometric functions), this is a serious drawback. Finally, the model is unstable with respect to fitting. The local coordinate frame rotates around the spine in the presence of torsion. Thus, small changes in the underlying spine can cause large changes in the shape of a cylinder with a non-circular cross section.

Terzopoulos et. al., developed the physically-based symmetry-seeking model [8] which is cylindrical in shape, and Sequiera employed a similar model for recovering vascular trees [5]. Our formulation differs from these in that we employ an analytic base cylinder model with mesh-like deformations from the surface rather than a model which is described solely by a spine and mesh.

Klok [1] Shani et. al., [6] devised cylinder models based on a series of discete frames which are interoplated to form a continuous model. These formualtions, however, do not permit the analytical computation of a reference frame at an

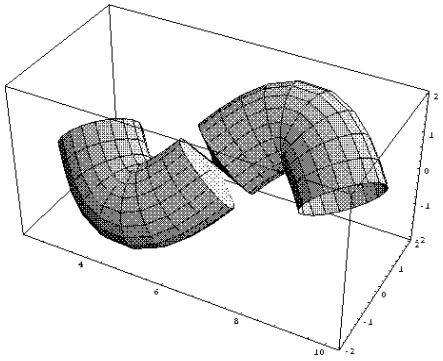

Fig. 3. A discontinuity in the cylinder based on the Frenet-Serret description due to an inflection point.

arbitrary point. In addition, their cross-section functions is not guaranteed to be orthogonal to the model's spine.

Finally, the EGC model proposed by O'Donnell et. al. [4], has a cross-section function orthogonal to the spine but the form the spine may take is quite limited. The spine must be expressible as a set of functions on an arbitrary axis in space. Loops, for example, are beyond its range.

In the context of past work, our model may be seen as a fusion of the Shani cylinder and the EGC. We use the B-spline based spine of Shani to create local coordinate frames at the B-spline's knot points. Rather than interpolating these frames as Shani did, however, we link these frames with a variation on the EGC. A more precise explanation is given in the next section.

3 Our Cylinder Formulation

Our model is based on a spine which is expressed in terms of cubic B-splines. B-splines are piecewise polynomial functions connected at knot points. Following Ballard, we calculate the tangents of the spine at the knot points and calculate the minimal rotations needed to align each tangent with the one following it. This series of rotations allows us to construct discrete frames at each of the knot points. We then interpolate between each of the frames using an EGC model. The EGC bases its coordinate system on the frames at either end of each span. The cross-section of the cylinder is plotted on the continuous frames provided by the EGC models. Finally local deformations away from this surface are described by a finite element mesh.

3.1 The Spine

The spine of our model is made up of $(n-1)$ piecewise cubic polynomial functions, $C_i(t)$, $i = 1, ..., (n-1)$, which are connected by n knot points, $(P_1 ... P_n)$. $C_i(t)$ may be calculated in terms of control points, $(V_1 ... V_n)$, and an intrinsic parameter t which runs $[0, 1)$ along each $C_i(t)$.

$$C_i(t) = \left[t^3\ t^2\ t\ 1\right] \cdot \mathbf{C} \cdot \mathbf{V}_i^T, \quad t \in [0,1), i = 1, ..., n-1 \tag{1}$$

where

$$\mathbf{C} = \frac{1}{6} \cdot \begin{vmatrix} -1 & 3 & -3 & 1 \\ 3 & -6 & 3 & 0 \\ -3 & 0 & 3 & 0 \\ 1 & 4 & 1 & 0 \end{vmatrix}$$

and $\mathbf{V}_i = [V_{i-1}\ V_i\ V_{i+1}\ V_{i+2}], \quad i = 1, ..., n-1$. Since the knot points appear at the beginning and end of every piecewise polynomial,

$$C_i(0) = P_i,$$
$$C_i(1) = P_{i+1}, \quad i = 1, ..., n-1$$

Thus the knot points may be represented as $P_i = \frac{1}{6}(V_{i-1} + 4V_i + V_{i+1})$. Assuming an open ended spine, we include two more constraints, increasing the number of control points by two,

$$V_0 = 2V_1 - V_2,$$
$$V_{n+1} = 2V_n - V_{n-1},$$

and using the array shorthands,

$$\mathbf{P} = [P_1, ..., P_n]$$
$$\mathbf{V} = [V_1, ..., V_n]$$

we can express the knot points in terms of the control points, $\mathbf{P} = [D] \cdot \mathbf{V}$. where

$$[D] = \frac{1}{6} \cdot \begin{vmatrix} 6 & & & & \\ 1 & 4 & 1 & & \\ & & \cdots & & \\ & & & 1 & 4\ 1 \\ & & & & 6 \end{vmatrix}.$$

We may then solve this linear system for the control points, plugging the results into Equation 1 to calculate the spine.

3.2 The Discrete Frames Along the Spine

At each of the knot points, $P_1 ... P_n$ we create a discrete trihedral frame by first computing the normalized tangents at each knot point, $A(P_i)$,

$$A(P_i) = \frac{dC_i(t)}{dt}, \quad i = 1..(n-1) \quad \text{at} \quad t = 0$$
$$A(P_n) = \frac{dC_{n-1}(t)}{dt} \quad \text{at} \quad t = 1$$

and determine the vector, F_i, orthogonal to each pair of tangents as we travel along the spine $F_i = A(P_i) \times A(P_{i+1})$ and the angle, α_i, around this vector which will align the tangents $\alpha_i = arccos(A(P_i) \cdot A(P_{i+1}))$.

We may then formulate the quaternions, Q_i, based on F_i and α_i, $i = 0, ..., n$. (We assume for $i = 0$ the transformation is from the unit Z vector to $A(P_1)$).

$$Q_i(\alpha_i, F_i) = (\cos(\frac{\alpha_i}{2}), \sin(\frac{\alpha_i}{2})F_i)$$

And define the concatenation of rotations in matrix form,

$$\mathbf{Q}_i = MatrixForm\left(\prod_{j=0}^{i-1} Q_j\right)$$

We then specify $\mathbf{L}_i$ as the translation of a point from the origin to the knot point, P_i. Then, the local coordinate frame at knot point P_i may be calculated by the transformation, $\mathbf{B}_i = \mathbf{Q}_i \cdot \mathbf{L}_i$.

Therefore, to calculate each of the successive frames, we apply a series of rotations to the unit Z vector (any starting vector is acceptable) followed by a translation to align this vector with the tangent at each of the knot points. The unit X vector may transformed with the same process to create a vector in the normal plane at each of the knots. It is these vectors which we will call M_i that will serve as the basis for aligning the EGCs on each span, $M_i = \mathbf{B}_i \cdot X$, $i = 1, ..., n$.

3.3 Interpolating Discrete Frames with EGCs

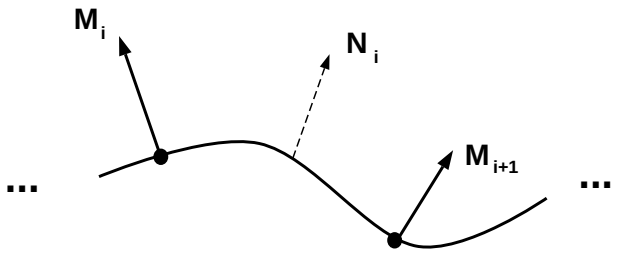

Fig. 4. The N_i vector is interpolated between the M_i and M_{i+1} vectors along the span.

For each span, C_i, $i = 1, ..., (n-1)$ the vector $N_i(t)$ is calculated.

$$N_i(t) = \mathbf{Q}_i \cdot Q(\alpha t, F) \cdot C_i(t)$$

N_i serves as a reference direction for calculating the frame along the span. It is aligned with M_i at the knot point corresponding to $t = 0$ and is linearly interpolated along the span such that it is aligned with the M_{i+1} at the knot point corresponding to $t = 1$.

$$N_i(0) = M_i$$
$$N_i(1) = M_{i+1}$$

A point, $K_i(t)$ in the plane orthogonal to the spine at $C_i(t)$ is calculated by finding the intersection of the line passing through $C_i(t)$ and $(C_i(t)+N_i(t))$ with the orthogonal plane (we drop the $_i$ and (t) for readability)

$$K = \begin{pmatrix} C_x + N_x - T_x^2 N_x - \\ T_x T_y N_y - T_x T_z N_z, \\ C_y - T_x T_y N_x + N_y - \\ T_y^2 N_y - T_y T_z N_z, \\ C_z - T_x T_z N_x - \\ T_y T_z N_y \\ + T_x^2 N_z + T_y^2 N_z \end{pmatrix}$$

where

$$T_i(t) = \frac{dC_i(t)}{dt}.$$

We then designate a unit direction, $U_i(t)$ (for up), as the normalized vector from $C_i(t)$ to $K_i(t)$, and $R_i(t)$ to be the cross product of U and $T_i(t)$.

$$U_i(t) = \frac{(K_i(t) - C_i(t))}{|(K_i(t) - C_i(t))|}, \qquad R_i(t) = U_i(t) \times T_i(t)$$

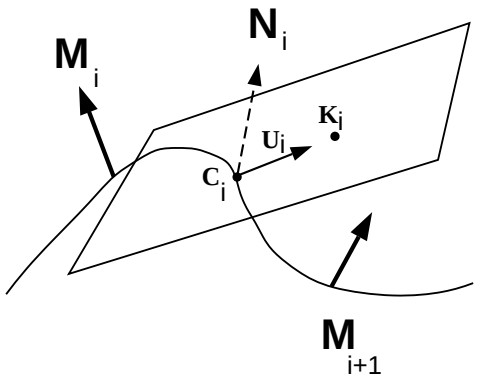

Fig. 5. Calculation of the vector U.

This forms a continuous unit trihedral frame upon which we may plot the cross-section function. It should be noted that the line passing thru $C_i(t)$ and $(C_i(t)+N_i(t))$ must intersect the plane orthogonal to the spine at $C_i(t)$ in order for this approach to work (i.e., it fails at $T_i(t) \cdot N_i(t) = 1$.

This anamoly is a very unusual case and may be tested for. It can be alleviated simply by calculating and including local frames at the offending points.

3.4 The Cross-section Function

We have chosen to implement an elliptical cross-section although any type of cross-section is permitted. The radial parameters, $radius1_i$ and $radius2_i$, $i = 1, ..., n$ are specified at the knot points and interpolated along the span. Thus a point on the span, $J_i(t, \theta)$, may be expressed as

$$J_i(t,\theta) = C_i(t) + r2_i(t)\cos(\theta)U_i(t) + r1_i(t)\sin(\theta)R_i(t)$$
$$\text{for } i = 1, ..., (n-1)$$

where

$$r1_i(t) = radius1_i(1-t) + radius1_{i+1}\ t$$
$$r2_i(t) = radius2_i(1-t) + radius2_{i+1}\ t$$

3.5 Local Deformations from the Surface

We have adopted a hybrid model formulation [7] in order to express fine detail while maintaining a gross description of the shape. Local displacements, $S_i(t, \theta)$, away from the model surface are interpolated via FEM shape functions based on the model's triangular element tessellation. In order to insure a smoothness of fit, this mesh-like component is endowed with a stretching penalty which penalizes sharp edges and insures that these local deformations do not describe features expressible by the base model.

4 Experimental Results

Recovery was performed using the physically-motivated approach of Metaxas and Terzopoulos [7]. All data was segmented via a 2-D dynamic programming method [2]. Figure 6 shows the final fit of the model to segmented healthy human aortic arch data taken from dense spiral CTA acquisition. The recovery required 60 iterations and reported the parameter values shown in Table 1.

In Figure 7 we show the lower portion of the aorta where an aneurysm has developed with fit information in Table 2. Note the increase in radius as we move up the cylinder.

5 Conclusions and Future Work

We have presented a novel cylinder formulation with an arbitrary spine and orthogonal cross-section and demonstrated its application in the medical domain.

In the future, we intend to employ rational B-splines allowing *any* rational space curve to serve as the spine. In addition, we will be adding a rotation component to the local coordinate systems and will allow the number of knot points to adaptively increase with respect to the data. Finally we are implementing bifurcations into the formulation and employing the model directly in image segmentation.

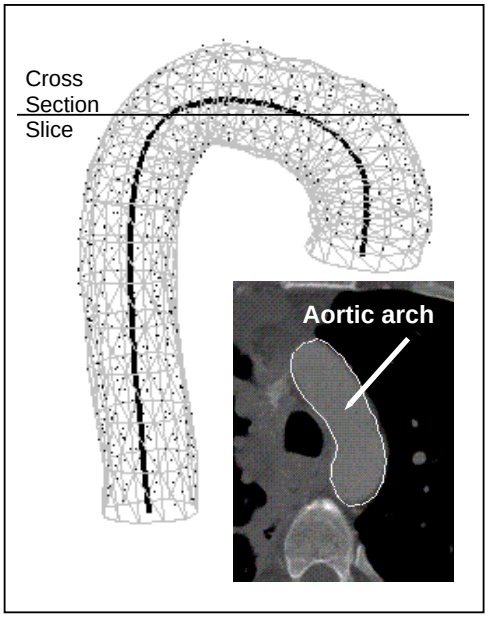

Fig. 6. The final fit of our model to segmented spiral CT angio data showing a healthy human aortic arch. Both the data points and the recovered centerline are shown in black. Inset: The superposition of the model on the original image data.

Fig. 7. Aorta with aneurysm.

Knot Points			Radii	
x	y	z	RadiusA	RadiusB
440.7	418.2	314.1	27.1	35.4
456.7	417.8	104.6	29.4	36.2
460.8	340.3	47.1	32.4	29.3
410.2	261.9	81.8	41.7	35.4
403.6	251.3	160.6	38.9	37.9
Surface Area: 25189.1 mm^2				

Table 1. Parameter values for a healthy aortic arch.

Knot Points			Radii	
x	y	z	RadiusA	RadiusB
106.8	95.1	182.3	10.5	10.6
105.7	96.6	188.2	11.3	11.6
107.9	96.1	196.5	10.6	11.5
109.4	94.4	205.6	7.3	8.2
119.3	93.2	217.9	7.6	7.5
119.4	93.1	224.8	7.1	6.4
118.1	91.9	232.6	5.4	6.1
117.8	90.5	240.0	5.4	4.8
115.6	89.7	247.6	5.3	5.6
115.2	87.4	255.0	4.3	4.9
Surface Area: 1413.3 mm^2				

Table 2. Parameter values for the diseased aorta. All values are in millimeters. Note the enormous increase in radii near the top of the model indicating an aneurysm.

References

1. f. Klok. Two moving coordinate frames for sweeping along a 3d trajectory. *Computer-Aided Geometric Design*, 3(3):217–229, November 1986.
2. A. Gupta, L von Kurowski, A. Singh, D. Geiger, C-C. Liang, M-Y. Chiu, L. P. Adler, M. Haacke, and D. L. Wilson. Cardiac mr image segmentation using deformable models. In *Proceedings of Conference on Computers in Cardiology*, pages 747–750. IEEE, 1993.
3. Q. Huang and G. C. Stockman. Generalized tube model: Recognizing 3d elongated objects from 2d intensity images. In *Proceedings of CVPR.*, pages 104–109. IEEE, 1993.
4. Thomas O'Donnell, Xi-Sheng Fang, Alok Gupta, and Terrance Boult. The extruded generalized cylinder: A deformable model for object recovery. In *Proceedings of the Conference on Computer Vision and Pattern Recognition*. IEEE, June 1994.
5. J. Sequiera, R. Ebel, and F. Scmitt. Three-dimensional modeling of tree-like anatomical structures. *Computerized Medical Imaging and Graphics*, 17:333–337, 1993.
6. U. Shani and D. Ballard. Splines as embeddings for generalized cylinders. *CVGIP: Image Understanding*, 27:129–156, 1984.
7. D. Terzopoulos and D. Metaxas. Dynamic 3D models with local and global deformations: Deformable superquadrics. *IEEE PAMI*, 13(7):703–714, 1991.
8. D. Terzopoulos, A. Witkin, and M. Kass. Constraints on deformable models: Recovering 3d shape and nonrigid motion. *Artificial Intelligence*, pages 91–123, August 1988.
9. Mourad Zerroug and Ramakant Nevatia. Quasi-invariant properties and 3-d shape recovery of non-straight, non-constant generalized cylinders. In *Proceedings of the CVPR*, pages 96–103. IEEE, 1993.

This article appeared in *IEEE CVPMED Conference on Computer Vision Virtual Reality and Rofiotics in Medicine*, 1997